 CMES, vol.15, no.3, pp.127-135, 2006

Local Defect Correction for the Boundary Element Method

G. Kakuba[1], R.M.M. Mattheij[2] and M.J.H. Anthonissen[3]

Abstract: This paper presents an efficient way to implement the Boundary Element Method (BEM) to capture high activity regions in a boundary value problem. In boundary regions where accuracy is critical, like in adaptive surface meshes, the method of choice is Local Defect Correction (LDC). We formulate the method and demonstrate its applicability and reliability by means of an example. Numerical results show that LDC and BEM together provide accurate solutions with less computational requirements given that BEM systems usually consist of dense matrices.

keyword: Local activity, Local defect correction, Global coarse grid, Local fine grid

1 Introduction

In the boundary element method, the solution of a function on a given domain is expressed as an integral equation in terms of its values and normal derivatives at the domain boundary. The boundary conditions are either Dirichlet or Neumann or both in the case of a mixed boundary conditions problem. Sometimes the boundary contains small regions of high activity. For example, for the Impressed Current Cathodic Protection Systems solved in Kakuba (2005), the boundary consists of small active regions there referred to as electrodes. In Pozrikidis (1992), a solution to a three-dimensional flow problem with a local region of high activity is also presented. In all these cases uniform grids have been used. For better accuracy with such localised regions of high activity, one usually has to employ a rather fine grid, either globally or as a composite grid. As discussed in Pozrikidis (2002), one way to circumvent local decreases in the accuracy of the BEM that occurs due to this local high activity is to use a high density of boundary elements globally. However, this results into extremely large systems that are computationally demanding especially in the case of BEM where matrices are usually dense. The advantages that BEM may have over FEM and FDM are then annihilated. In this paper we show how to circumvent this by incorporating LDC into BEM in the case of localised regions that require a high density of elements. This local high activity might be caused by the differential operator itself, the forcing terms in the differential equation, the boundary conditions or by an irregular boundary. Shiah, Guao and Tan in Shiah, Guao, and Tan (2005) discuss two dimensional BEM thermoelastic analysis of boundary value problems with concentrated heat sources which are often placed at the surface of the domain for many practical applications. The discretisation of such problems involves applying many refined elements in the vicinity of the source that leads to large composite grid matrices. Such problems could be solved computationally cheaper by using LDC as we shall demonstrate in this paper.

In Ferket and Reusken (1996), a special case of the LDC method that was introduced in Hackbusch (1984) is analysed using finite difference discretisations. In Anthonissen (2001) LDC techniques are well analysed for finite difference and finite volume methods and some applications are also discussed. In this article we extend the LDC method for use with BEM. In general, a uniform grid can be either too computationally expensive if it is too fine, or inaccurate, if it is coarse, Ma, Lu, and Komanduri (2005). A non-uniform grid with refinement can provide accurate results while minimising the overall computational time. This is what LDC does. In the LDC method a fine grid solution is used to overall improve the coarse grid approximation. This is achieved through a so-called defect correction in which the fine grid solution is used to approximate the local discretisation error of the coarse grid. We give a brief development of the BEM and explain local defect correction. We combine BEM and LDC in an algorithm that we shall call a BEM-LDC algorithm. Numerical experiments are carried out using a suitable example and results discussed. The results show that we can reduce the complexity of

[1] TU Eindhoven, CASA. Email: g.a.kakuba@tue.nl.
[2] TU/e CASA.
[3] TU/e CASA.

the solution method by at least a factor two while keeping a good accuracy. For instance, in the particular case of the problems that have been solved in Kakuba (2005), the use of BEM-LDC would reduce the complexity by at least a factor 40!

The paper is built up as follows: in the next section, Section 2, we give a brief description of BEM and explain the LDC algorithm for BEM. In particular, in Section 2.1, a brief account of BEM formulation is given. The local problem and local defect are explained in Sections 2.2 and 2.3 respectively. In Section 2.4, we describe defect correction and present the BEM-LDC algorithm. Section 3 brings all the previous sections together by discussing some numerical experiments and their results. The last section, Section 4, will be devoted to conclusions.

2 Boundary Element Method with Local Defect Correction

In this section we explain the development of the BEM-LDC algorithm. A brief description of the BEM formulation is presented. We give an account of the LDC technique and then show how we combine BEM and LDC together to get a better solution to a boundary value problem.

2.1 Boundary Element Method, a First Approximation of the Solution

Let us consider the potential problem governed by the Laplace equation and given by the boundary value problem

$$\begin{cases} \nabla^2 u(\boldsymbol{r}) = 0 & \boldsymbol{r} \in \Omega, \\ u(\boldsymbol{r}) = g_1(\boldsymbol{r}) & \boldsymbol{r} \in \partial\Omega_1, \\ \dfrac{\partial u}{\partial n}(\boldsymbol{r}) := q(\boldsymbol{r}) = g_2(\boldsymbol{r}) & \boldsymbol{r} \in \partial\Omega \backslash \partial\Omega_1, \end{cases} \tag{1}$$

where $\partial\Omega$ denotes the boundary of the problem domain Ω. For a smooth boundary, the integral equation is, see Paris and Canas (1997), Pozrikidis (1992),

$$\frac{1}{2}u(\boldsymbol{r}) = \int_{\partial\Omega} u(\boldsymbol{r}')\frac{\partial v}{\partial n}(\boldsymbol{r}';\boldsymbol{r})\,dS(\boldsymbol{r}') - \int_{\partial\Omega} v(\boldsymbol{r}';\boldsymbol{r})\frac{\partial u}{\partial n}(\boldsymbol{r}')\,\mathrm{d}S(\boldsymbol{r}'), \quad \boldsymbol{r} \in \partial\Omega. \tag{2}$$

The surface $\partial\Omega$ is divided into N elements; in this paper we use constant triangular elements. Thus, on each of the elements $i = 1,2,\ldots,N$, we assume that the functions u and q remain constant. We introduce the notation u^i, q^i and $\partial\Omega_j$ to denote $u(\mathbf{r}_i), q(\mathbf{r}_i)$ and the $j-$th triangle respectively. Discretising Eq. (2) and letting the fixed point $\mathbf{r}$ to be the collocation point at element i, we get

$$\frac{1}{2}u^i - \sum_{j=1}^{N} u^j \int_{\partial\Omega_j} \frac{\partial v}{\partial n}(\boldsymbol{r}';\boldsymbol{r}_i)\,\mathrm{d}S(\boldsymbol{r}') = -\sum_{j=1}^{N} q^j \int_{\partial\Omega_j} v(\boldsymbol{r}';\boldsymbol{r}_i)\,\mathrm{d}S(\boldsymbol{r}'). \tag{3}$$

Writing (3) for all the elements $i = 1,2,\ldots,N$, the resulting equations can be written in matrix form as

$$\mathbf{Fu} = \mathbf{Gq}, \tag{4}$$

where

$$F_{ij} = \hat{F}_{ij} - \frac{1}{2}\delta_{ij},\ \hat{F}_{ij} = \int_{\partial\Omega_j} \frac{\partial v}{\partial n}(\boldsymbol{r}';\boldsymbol{r}_i)\,\mathrm{d}S(\boldsymbol{r}') \tag{5}$$

and

$$G_{ij} = \int_{\partial\Omega_j} v(\boldsymbol{r}';\boldsymbol{r}_i)\,\mathrm{d}S(\boldsymbol{r}'). \tag{6}$$

Applying boundary conditions to (4) results into the system

$$\mathbf{A}^{\mathrm{H}}\mathbf{x}^{\mathrm{H}} = \mathbf{b}^{\mathrm{H}} \tag{7}$$

where $\mathbf{x}^{\mathrm{H}}$ contains the unknown values of u and q. Solving this system gives us an initial approximation $\mathbf{x}_0^{\mathrm{H}}$. The superscript H denotes the solution on a coarse grid (grid size H). Therefore $\mathbf{x}_0^{\mathrm{H}}$ is the initial solution in the nodes when we have a coarse mesh everywhere.

Now assume that the continuous solution u of Eq. (32) has a high activity region in some (small) part of the domain boundary. This high activity of u may be captured by discretising Eq. (2) on a composite grid. To this end, we choose $\partial\Omega_{\mathrm{l}} \subset \partial\Omega$ such that the high activity of u is contained in $\partial\Omega_{\mathrm{l}}$. In $\partial\Omega_{\mathrm{l}}$, we choose a local fine grid (grid size h), which we denote by $\partial\Omega_{\mathrm{l}}^{\mathrm{h}}$. The fine grid is chosen such that $\partial\Omega^{\mathrm{H}} \cap \partial\Omega_{\mathrm{l}} \subset \partial\Omega_{\mathrm{l}}^{\mathrm{h}}$, i.e., element nodes of the global coarse grid that lie in the area of refinement are nodes of the local fine grid too.

When Eq. (2) has been discretised and solved on a coarse grid, and when an area of the coarse grid has been refined and a local solution has been calculated on the finer

grid solution, we can use the local fine grid to update the coarse grid approximation.

Suppose $\mathbf{x}^*$ is the exact solution, then substitution in Eq. (7) would give

$$\mathbf{A}^{\mathrm{H}}\mathbf{x}^* = \mathbf{b}^{\mathrm{H}} + \mathbf{d}^{\mathrm{H}} \tag{8}$$

where the defect $\mathbf{d}^{\mathrm{H}}$ is a vector of the local discretisation errors. If we knew the values of the defect $\mathbf{d}^{\mathrm{H}}$, we could add them to the right hand side of Eq. (7) and solve this system of equations to find the exact values of u and q in (4).

2.2 *The Local Problem*

Since the exact solution is normally unknown, we cannot calculate $\mathbf{d}^{\mathrm{H}}$ in Eq. (8). What we can do though is to use the approximation calculated on the local fine grid to estimate $\mathbf{d}^{\mathrm{H}}$ for those grid elements of the global coarse grid that lie within $\partial\Omega_{\mathrm{l}}$. To formulate the local problem, we form a composite grid wherein we have a fine grid in the local region whereas we maintain the coarse grid elsewhere. We then apply the discretised integral equation Eq. (3) to the composite grid. Therefore, in Eq. (7), we now denote the operator $\mathbf{A}^{\mathrm{H}}$ as $\mathbf{A}^{\mathrm{H,h}}$ and the vectors $\mathbf{x}^{\mathrm{H}}$ and $\mathbf{b}^{\mathrm{H}}$ are split in such a way that we can write,

$$\mathbf{A}^{\mathrm{H,h}} \begin{pmatrix} \mathbf{x}_{\mathrm{c}}^{\mathrm{H}} \\ \mathbf{x}_{\mathrm{l}}^{\mathrm{h}} \end{pmatrix} = \begin{pmatrix} \mathbf{f}^{\mathrm{H}} \\ \mathbf{f}_{\mathrm{l}}^{\mathrm{h}} \end{pmatrix}, \tag{9}$$

where the subscripts c and l are used to mean that $\mathbf{x}_{\mathrm{c}}^{\mathrm{H}}$ is the solution vector in the nodes that lie outside the (local) active region where we have the coarse mesh and $\mathbf{x}_{\mathrm{l}}^{\mathrm{h}}$ the solution in the nodes that lie in the local region where we have the fine mesh. Analogously, let us split the operator $\mathbf{A}^{\mathrm{H,h}}$ so that Eq. (9) can be written as

$$\begin{pmatrix} \mathbf{A}_{\mathrm{c}}^{\mathrm{H}} & \mathbf{B}_{\mathrm{c,l}}^{\mathrm{H,h}} \\ \mathbf{C}_{\mathrm{l,c}}^{\mathrm{H,h}} & \mathbf{A}_{\mathrm{l}}^{\mathrm{h}} \end{pmatrix} \begin{pmatrix} \mathbf{x}_{\mathrm{c}}^{\mathrm{H}} \\ \mathbf{x}_{\mathrm{l}}^{\mathrm{h}} \end{pmatrix} = \begin{pmatrix} \mathbf{f}^{\mathrm{H}} \\ \mathbf{f}_{\mathrm{l}}^{\mathrm{h}} \end{pmatrix}. \tag{10}$$

From Eq. (10) we extract two equations:

$$\mathbf{C}_{\mathrm{l,c}}^{\mathrm{H,h}}\mathbf{x}_{\mathrm{c}}^{\mathrm{H}} + \mathbf{A}_{\mathrm{l}}^{\mathrm{h}}\mathbf{x}_{\mathrm{l}}^{\mathrm{h}} = \mathbf{f}_{\mathrm{l}}^{\mathrm{h}}, \tag{11a}$$

$$\mathbf{A}_{\mathrm{c}}^{\mathrm{H}}\mathbf{x}_{\mathrm{c}}^{\mathrm{H}} + \mathbf{B}_{\mathrm{c,l}}^{\mathrm{H,h}}\mathbf{x}_{\mathrm{l}}^{\mathrm{h}} = \mathbf{f}^{\mathrm{H}}. \tag{11b}$$

Having added more elements in the local region, see Figs. 1 and 2, we rewrite Eq. (11a) in the form

$$\mathbf{A}_{\mathrm{l}}^{\mathrm{h}}\mathbf{x}_{\mathrm{l}}^{\mathrm{h}} = \mathbf{f}_{\mathrm{l}}^{\mathrm{h}} - \mathbf{C}_{\mathrm{l,c}}^{\mathrm{H,h}}\mathbf{x}_{\mathrm{c}}^{\mathrm{H}}. \tag{12}$$

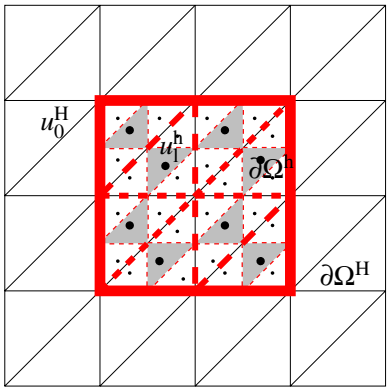

Fig. 1 : A composite grid discretisation: The thick continuous rectangle encloses the active region, the large dots on the shaded triangles indicate nodes that belong to $\partial\Omega_{\mathrm{l}}^{\mathrm{H}}$. The thick dashed mesh shows the triangles of the coarse grid that belong to the active region.

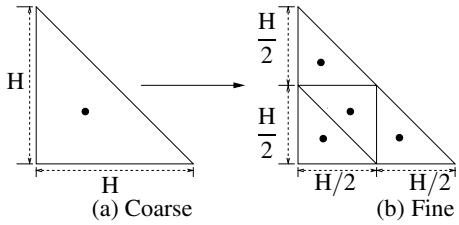

Fig. 2 : At each refinememnt step, a coarse triangle is divided into four.

We split the initial global coarse grid solution $\mathbf{x}_0^{\mathrm{H}}$ in the form $\left(\mathbf{x}_{\mathrm{c},0}^{\mathrm{H}}\ \mathbf{x}_{\mathrm{l},0}^{\mathrm{H}}\right)$ where $\mathbf{x}_{\mathrm{c},0}^{\mathrm{H}}$ is the solution in the nodes of the global coarse grid that lie outside the local region and $\mathbf{x}_{\mathrm{l},0}^{\mathrm{H}}$ is the solution in the nodes of the global coarse grid that lie in the local region. Similar vector partitionings in the sequel are analogously defined. We then substitute $\mathbf{x}_{\mathrm{c},0}^{\mathrm{H}}$ for $\mathbf{x}_{\mathrm{c}}^{\mathrm{H}}$ in Eq. (12) and hence obtain the following system of equations for the local problem:

$$\mathbf{A}_{\mathrm{l}}^{\mathrm{h}}\mathbf{x}_{\mathrm{l},0}^{\mathrm{h}} = \mathbf{f}_{\mathrm{l}}^{\mathrm{h}} - \mathbf{C}_{\mathrm{l,c}}^{\mathrm{H,h}}\mathbf{x}_{\mathrm{c},0}^{\mathrm{H}} = \mathbf{b}_{\mathrm{l}}^{\mathrm{h}}. \tag{13}$$

Thus we form a local problem in such a way that outside the local region, the solution is known and is the global coarse grid solution. This results in a smaller system that is cheaply solved to yield the local problem initial solution $\mathbf{x}_{\mathrm{l},0}^{\mathrm{h}}$, which is the solution in the nodes of the composite grid that lie in the local region where we have the fine mesh.

The refinement strategy is similar to that discussed

in Ferket and Reusken (1996) where it is referred to as *local uniform grid refinement*. The mesh size of the global coarse grid is chosen in agreement with the smooth behaviour of the solution outside the high activity region. Besides a global grid, a local grid is used which is also uniform. The local grid covers only a small part of the domain and contains the high activity region. The grid size of this local region is also chosen in agreement with the behaviour of the solution in that region. Ideas are also drawn from the refinement strategy used in Boersma, Kooper, Niewstadt, and Wesseling (1997) where they discuss local grid refinement in large-eddy simulations. The purpose of local grid refinement is then to obtain a better resolution of turbulence in areas which are considered critical in terms of the total flow problem.

2.3 The local defect

In the constant elements discretisation, the values of the functions on a particular element are associated with the centroids of the triangles which are called nodes. Let k denote a triangle node. Let us partition the elements of the coarse grid as

$$\partial\Omega^{\mathrm{H}} = \partial\Omega_{\mathrm{l}}^{\mathrm{H}} \cup \partial\Omega_{c}^{\mathrm{H}}, \tag{14}$$

where $\partial\Omega_{\mathrm{l}}^{\mathrm{H}} := \{k \in \partial\Omega^{\mathrm{H}} | k \in \partial\Omega_{\mathrm{l}}\}$, $\partial\Omega_{\mathrm{c}}^{\mathrm{H}} := \partial\Omega^{\mathrm{H}} \backslash \partial\Omega_{\mathrm{l}}^{\mathrm{H}}\}$. If u^* and q^* denote the exact values of u and q respectively, then we would have the local discretisation errors given by, from Eq. (3),

$$\begin{aligned} d_i &:= \sum_{j=1}^{N} u_j^* \int_{\partial\Omega_j} \frac{\partial v}{\partial n}(\mathbf{r}';\mathbf{r}_i)\,\mathrm{d}S(\mathbf{r}') \\ &\quad - \sum_{j=1}^{N} q_j^* \int_{\partial\Omega_j} v(\mathbf{r}';\mathbf{r}_i)\,\mathrm{d}S(\mathbf{r}') - \frac{1}{2}u_i^* \\ &= \sum_{j=1}^{N} (\hat{F}_{ij} - \frac{1}{2}\delta_{ij})u_j^* - \sum_{j=1}^{N} q_j^* G_{ij} \\ &= \sum_{j=1}^{N} F_{ij}u_j^* - \sum_{j=1}^{N} q_j^* G_{ij}, \mathbf{r}_i \in \partial\Omega^{\mathrm{H}}. \end{aligned} \tag{15}$$

Applying boundary conditions, Eq. (15) yields

$$d_i = \sum_{j=1}^{N} A_{ij}x_j^* - b_i, \quad \mathbf{r}_i \in \partial\Omega^{\mathrm{H}}. \tag{16}$$

If we write Eq.(16) for all $\mathbf{r}_i \in \partial\Omega_{\mathrm{l}}^{\mathrm{H}}$, we obtain the following local defect on $\partial\Omega_{\mathrm{l}}^{\mathrm{H}}$, in vector form

$$\mathbf{d}_{\mathrm{l}}^{\mathrm{H}} = \mathbf{A}_{\mathrm{ld}}^{\mathrm{H}}\mathbf{x}_{\mathrm{ld}}^{*\mathrm{H}} - \mathbf{b}_{\mathrm{l}}^{\mathrm{H}}. \tag{17}$$

Here, $x^{*\mathrm{H}}$ is the projection on $\partial\Omega^{\mathrm{H}}$ of the exact solution and the subscript ld is used to denote local defect. We can partition the matrix $\mathbf{A}_{\mathrm{ld}}^{\mathrm{H}}$ into the form

$$\mathbf{A}_{\mathrm{ld}}^{\mathrm{H}} = \begin{pmatrix} \mathbf{C}_{\mathrm{l,c}}^{\mathrm{H}} & \mathbf{A}_{\mathrm{l}}^{\mathrm{H}} \end{pmatrix} \tag{18}$$

so that we have

$$\mathbf{d}_{\mathrm{l}}^{\mathrm{H}} = \mathbf{C}_{\mathrm{l,c}}^{\mathrm{H}}\mathbf{x}_{\mathrm{c}}^{*\mathrm{H}} + \mathbf{A}_{\mathrm{l}}^{\mathrm{H}}\mathbf{x}_{\mathrm{l}}^{*\mathrm{H}} - \mathbf{b}_{\mathrm{l}}^{\mathrm{H}}, \tag{19}$$

where $\mathbf{x}^{*\mathrm{H}} = \begin{pmatrix} \mathbf{x}_{\mathrm{l}}^{*\mathrm{H}} & \mathbf{x}_{c}^{*\mathrm{H}} \end{pmatrix}$ and $\mathbf{x}_{\mathrm{l}}^{*\mathrm{H}}$ and $\mathbf{x}_{c}^{*\mathrm{H}}$ are the projections of $\mathbf{x}^{*\mathrm{H}}$ onto $\partial\Omega_{\mathrm{l}}^{\mathrm{H}}$ and $\partial\Omega_{c}^{\mathrm{H}}$ respectively.

Since we do not know the exact solution $\mathbf{x}^*$, we cannot calculate $\mathbf{d}_{\mathrm{l}}^{\mathrm{H}}$ using (19). What we can do though, is to use the approximation $\mathbf{x}_{\mathrm{l},0}^{\mathrm{h}}$ calculated on the local fine grid to estimate $\mathbf{d}_{\mathrm{l}}^{\mathrm{H}}$. Using Eq. (19), we find

$$\begin{aligned} \mathbf{d}_{\mathrm{l}}^{\mathrm{H}} &= \mathbf{C}_{\mathrm{l,c}}^{\mathrm{H}}\mathbf{x}_{\mathrm{c}}^{*\mathrm{H}} + \mathbf{A}_{\mathrm{l}}^{\mathrm{H}}x_{\mathrm{l}}^{*\mathrm{H}} - \mathbf{b}_{\mathrm{l}}^{\mathrm{H}} \\ &\approx \mathbf{C}_{\mathrm{l,c}}^{\mathrm{H}}\mathbf{x}_{\mathrm{c},0}^{\mathrm{H}} + \mathbf{A}_{\mathrm{l}}^{\mathrm{H}}R^{\mathrm{H,h}}\mathbf{x}_{\mathrm{l},0}^{\mathrm{h}} - \mathbf{b}_{\mathrm{l}}^{\mathrm{H}} \\ &:= \mathbf{d}_{\mathrm{l},0}^{\mathrm{H}}. \end{aligned} \tag{20}$$

Here we have introduced the operator $R^{\mathrm{H,h}}$ which is the restriction from $\partial\Omega_{\mathrm{l}}^{\mathrm{h}}$ onto $\partial\Omega_{\mathrm{l}}^{\mathrm{H}}$.

2.4 The Defect correction and the BEM-LDC Algorithm

In light of Eq. (19) and Eq. (20), we partition the matrix $\mathbf{A}^{\mathrm{H}}$ in Eq. (7) into the form

$$\mathbf{A}^{\mathrm{H}} = \begin{pmatrix} \mathbf{A}_{\mathrm{c}}^{\mathrm{H}} & \mathbf{B}_1 \\ \mathbf{B}_2 & \mathbf{A}_{\mathrm{l}}^{\mathrm{H}} \end{pmatrix}. \tag{21}$$

The vectors $\mathbf{x}^{\mathrm{H}}$ and $\mathbf{b}^{\mathrm{H}}$ are also partitioned accordingly so that Eq. (7) can be rewritten as

$$\begin{pmatrix} \mathbf{A}_{\mathrm{c}}^{\mathrm{H}} & \mathbf{B}_1 \\ \mathbf{B}_2 & \mathbf{A}_{\mathrm{l}}^{\mathrm{H}} \end{pmatrix} \begin{pmatrix} \mathbf{x}_{\mathrm{c}}^{\mathrm{H}} \\ \mathbf{x}_{\mathrm{l}}^{\mathrm{H}} \end{pmatrix} = \begin{pmatrix} \mathbf{b}_{\mathrm{c}}^{\mathrm{H}} \\ \mathbf{b}_{\mathrm{l}}^{\mathrm{H}} \end{pmatrix}. \tag{22}$$

Using Eq. (20) we find an estimate of the local discretisation error of the coarse grid discretisation at all points of $\partial\Omega_{\mathrm{l}}^{\mathrm{H}}$. Therefore, we can update the coarse grid approximation by placing the estimate in Eq. (20) at the right hand side of the coarse grid Eq. (7) or Eq. (22). This leads to the coarse grid correction step to find $\mathbf{x}_i^{\mathrm{H}}, i = 1,$ on the coarse grid:

$$\begin{aligned} \mathbf{A}^{\mathrm{H}}\mathbf{x}_i^{\mathrm{H}} &= \begin{pmatrix} \mathbf{b}_{\mathrm{c}}^{\mathrm{H}} \\ \mathbf{b}_{\mathrm{l}}^{\mathrm{H}} + \mathbf{d}_{\mathrm{l},i-1}^{\mathrm{H}} \end{pmatrix} \\ &= \begin{pmatrix} \mathbf{b}_{\mathrm{c}}^{\mathrm{H}} \\ \mathbf{C}_{\mathrm{l,c}}^{\mathrm{H}}\mathbf{x}_{\mathrm{c},0}^{\mathrm{H}} + \mathbf{A}_{\mathrm{l}}^{\mathrm{H}}R^{\mathrm{H,h}}\mathbf{x}_{\mathrm{l},0}^{\mathrm{h}} \end{pmatrix}. \end{aligned} \tag{23}$$

In Anthonissen (2001), it is shown that it might be beneficial to use the estimate Eq. (20) not at all nodes but exclude those that lie close to the interface between the active region and the rest of the boundary. However in this paper this idea has not been used. Once we have identified the active region, we refine it all and calculate the defect there without putting distance between it and the rest of the boundary. Because Eq. (23) incorporates estimates of the local discretisation error of the coarse grid discretisation, the new solution $\mathbf{x}_1^{\mathrm{H}}$ is assumed to be more accurate than $\mathbf{x}_0^{\mathrm{H}}$. Hence a solution based on the new approximation $\mathbf{x}_1^{\mathrm{H}}$ provides a better boundary condition for the local problem. A better solution on the local fine grid can be found as before by solving Eq. (13) with $\mathbf{x}_{1,1}^{\mathrm{h}}$. In summary we have the following algorithm:

Algorithm 1, BEM-LDC Algorithm

- Initialisation
  - Solve the basic coarse grid problem Eq. (7)
  - Solve the local fine grid problem Eq. (13) with $i = 0$.
- Iterations $i = 1, 2, \ldots$
  - Solve the updated coarse grid problem Eq. (23)
  - Solve the local fine grid problem Eq. (13)

3 Numerical experiments

3.1 Test example

Consider the following exterior potential problem:

$$\begin{cases} \nabla^2 u(\boldsymbol{r}) = 0 & \boldsymbol{r} \in \Omega = \mathcal{R}^3 \backslash \Omega^c, \\ u(\boldsymbol{r}) = \dfrac{1}{r} & \boldsymbol{r} \in \partial\Omega \backslash \partial\Omega_1, \\ \dfrac{\partial u}{\partial n}(\boldsymbol{r}) := q(\boldsymbol{r}) = \dfrac{\partial}{\partial n}\left(\dfrac{1}{r}\right) & \boldsymbol{r} \in \partial\Omega_1, \end{cases} \tag{24}$$

where $u(\boldsymbol{r})$ behaves at most as $O(R^{-1})$ as $R \to \infty$, R the distance from a point on $\partial\Omega \cup \partial\Omega_1$, and

$$r = ||\boldsymbol{r} - \boldsymbol{r}_0||, \ \boldsymbol{r} = (x, y, z), \tag{25}$$

$$\Omega^c = \{\boldsymbol{r} : \boldsymbol{r} \in [0,4] \times [0,10] \times [0,6]\}, \tag{26}$$

$$\partial\Omega_1 = \{\boldsymbol{r} : x = 4.0\}, \tag{27}$$

$$u = 1/r. \tag{28}$$

That is, for this problem we know the analytic solution and we can therefore compute the errors. Let $\mathbf{e} = \mathbf{u} - \tilde{\mathbf{u}}$, where $\tilde{\mathbf{u}}$ is the numerical solution and $\mathbf{u}$ the exact solution, denote the error vector in estimating $\mathbf{u}$. In Eq. (25), let $\boldsymbol{r}_0 = (3.7, 5.0, 3.0)$. Solving the problem on the coarse grid using BEM with a uniform distribution of elements, we find that $||\mathbf{e}_0||_\infty = 0.5544$ for H = 1.0 (496 elements) whereas $||\mathbf{e}_0||_\infty = 0.2589$ for H = 0.5 (1984 elements), where $\mathbf{e}_0 = \mathbf{u} - \tilde{\mathbf{u}}_0$. Using the BEM-LDC algorithm with $h = 0.5$, the updated coarse grid solution error is $||\mathbf{e}_1||_\infty = 0.1385677$. This is a good promise.

Fixing $\boldsymbol{r}_0 = (3.7, 5.0, 3.0)$ creates a region of high activity on the surface $\partial\Omega$ around the point $\boldsymbol{r} = (4.0, 5.0, 3.0)$. Let the local active region be

$$\partial\Omega_1 = \{(x, y, z) : x = 4.0, 4.0 \le y \le 6.0, 2.0 \le z \le 4.0\}. \tag{29}$$

To futher analyse results of the BEM-LDC algorithm, we have increased the activity by setting $\boldsymbol{r}_0 = (3.9, 5.0, 3.0)$ and solved the boundary value problem Eq. (24). The results obtained are presented in Tab. 1 and in figures Fig. 3 to Fig. 6. The figures Fig. 7 to Fig. 10 show the evolution of the grid used in this example. The matrix size of the coarse grid problem is 496. The matrix size of the local problem is denoted S_1 and $N_{\mathrm{a}}^{\mathrm{H}}$, the number of coarse grid elements in the active region, is 8.

Tab. 1 : Uniform coarse grid errors ($||\mathbf{e}_0^{\mathrm{H}}||_\infty$) and errors after the first, second and third iterations of the BEM-LDC Algorithm, $N_{\mathrm{a}}^{\mathrm{H}} = 8$.

H	1.0	1.0	1.0
h	0.500	0.250	0.125
$\|\|\mathbf{e}_0^{\mathrm{H}}\|\|_\infty$	1.416616	1.416616	1.416616
$\|\|\mathbf{e}_1\|\|_\infty$	0.747629	0.395171	0.393202
$\|\|\mathbf{e}_2\|\|_\infty$	0.740818	0.394991	0.392970
$\|\|\mathbf{e}_3\|\|_\infty$	0.740818	0.394989	0.392966
S_1	32	128	512

In Tab. 1, using a uniform grid would have resulted into a system of size 1984, 7936 and 31744 respectively for h= 0.5, 0.25 and 0.125! In the case of a composite grid solution, the systems would have sizes 520, 616 or 1000 respectively. We note from the table that the algorithm

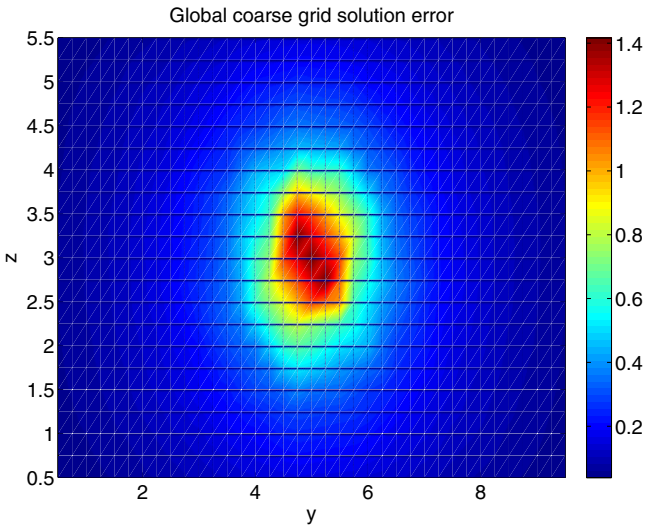

Fig. 3 : Uniform global coarse grid error on the surface $\{(x,y,z) : x = 4.0, 0 \le y \le 10.0, 0 \le z \le 6.0\}$.

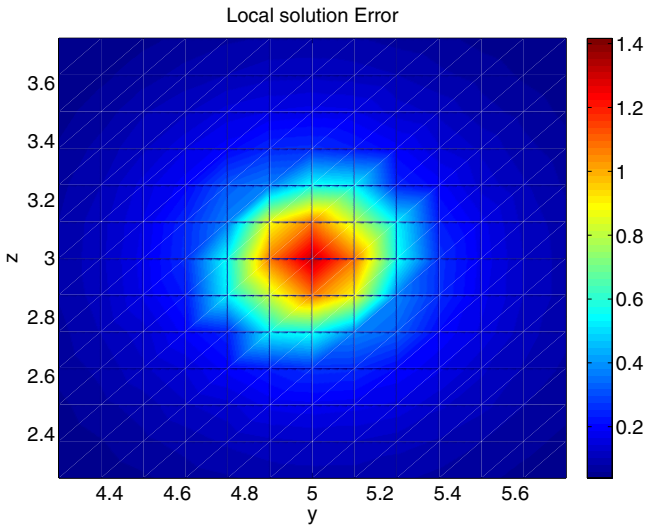

Fig. 4 : The local problem solution error in the local active region $\{(x,y,z) : x = 4.0, 4.0 \le y \le 6.0, 2.0 \le z \le 4.0\}$

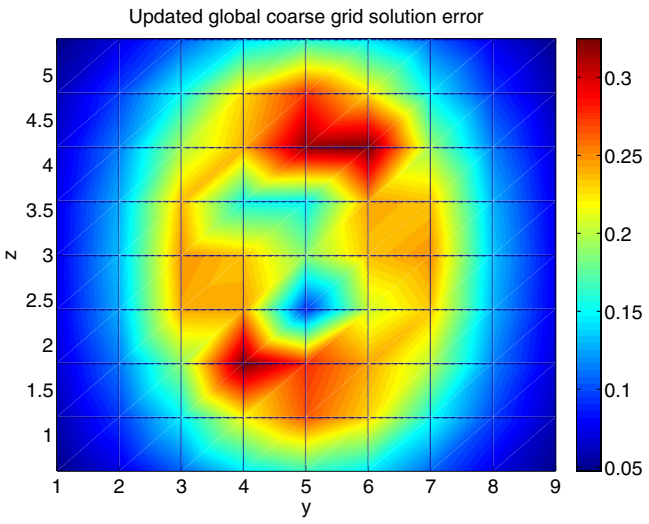

Fig. 5 : Updated global coarse grid error on the surface $\{(x,y,z) : x = 4.0, 0 \le y \le 10.0, 0 \le z \le 6.0\}$.

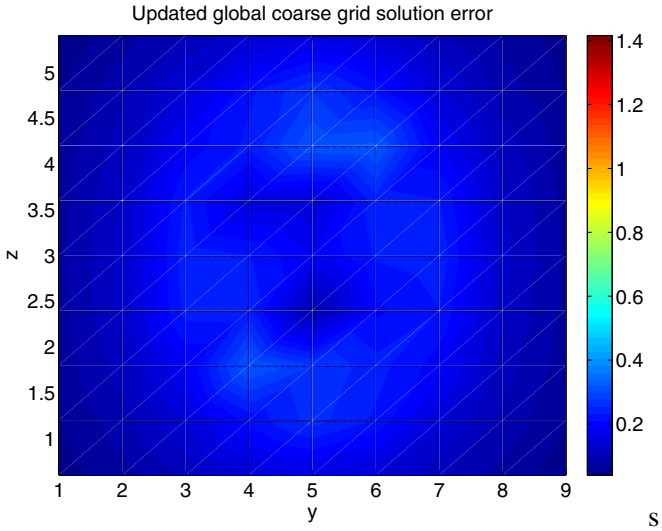

Fig. 6 : The updated global coarse grid solution error ploted on the same colour scale as in Fig. 3 and Fig. 4.

converges in one step which involves solving two global coarse grid size problems and one local problem.

Let N be the size of the global problem and M the size of the local problem. We assume that the local region is only a small part of the domain such that $N - N_a^H \approx N$, i.e., $N_a^H \ll N$. For example, in our experiments, $N = 496$ and $N_a^H = 8$. The operational count for LU-decomposition is $\frac{1}{3}N^3$ for a size N matrix. After refinement, we have a composite problem of complexity

$$\frac{1}{3}(N+M)^3 \approx \frac{8}{3}N^3 \text{ if } M \approx N. \tag{30}$$

The BEM-LDC algorithm converges in one step and has total complexity

$$2 \cdot \frac{1}{3}N^3 + \frac{1}{3}M^3 \approx N^3. \tag{31}$$

Comparing Eq. (30) and Eq. (31) clearly shows that the BEM-LDC algorithm is at least twice less complex than solving the composite problem.

With the same coarse grid problem, if we were to refine globally in the same procedure as illustrated in Fig. 2, then achieving a grid of H= 0.125 would result in a sys-

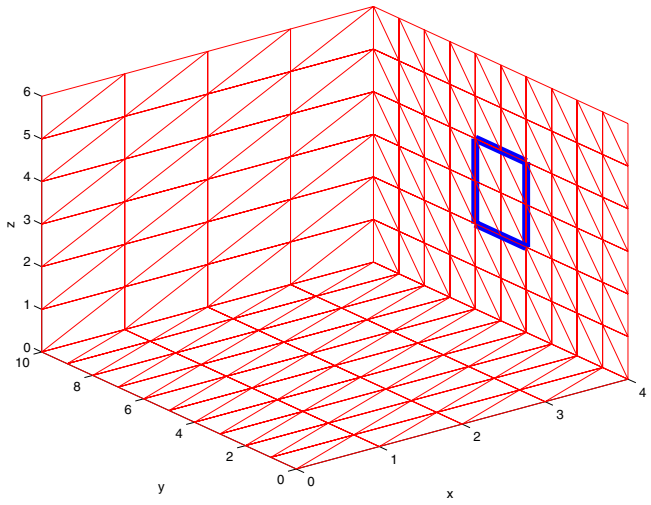

Fig. 7 : Uniform global coarse grid of size H=1.0, only three faces shown for clarity. The active region on the face $x = 4.0$ is marked with the thick rectangle.

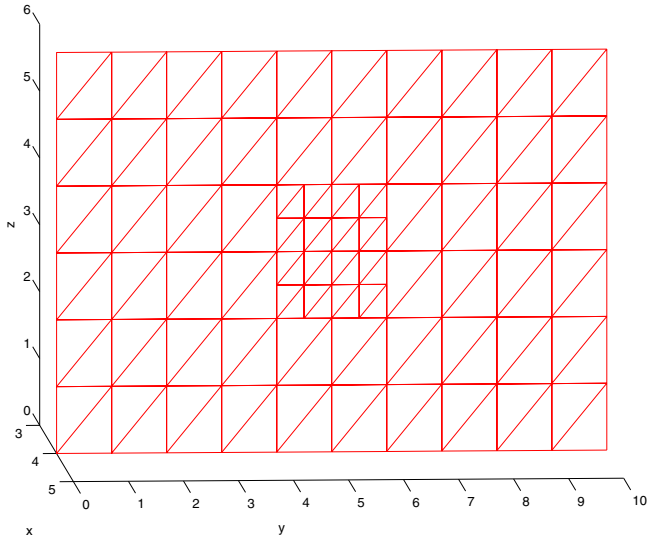

Fig. 8 : The composite grid, only the face $x = 4.0$ is shown. The active region has been refined to a grid of size h=0.5.

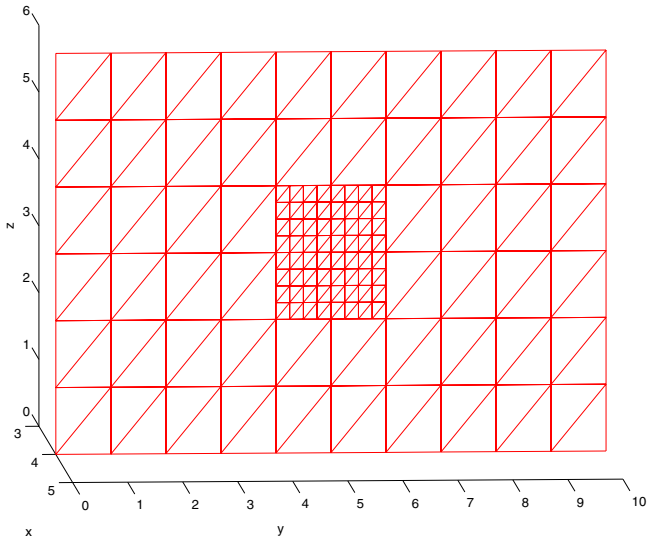

Fig. 9 : The composite grid on the face $x = 4.0$ with the active region refined to a grid of size h=0.25.

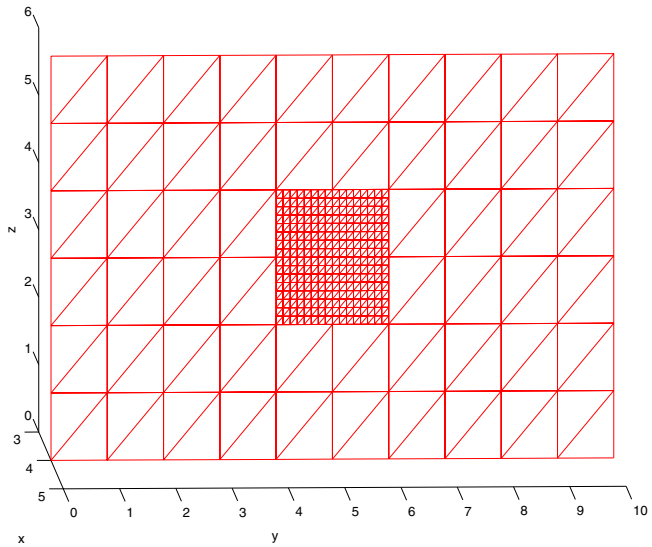

Fig. 10 : The composite grid on the face $x = 4.0$ with the active region refined to a grid of size h=0.125.

tem of size $128N$ with a complexity of $\frac{1}{3}(128N)^3$. Another pay-off when we use the BEM-LDC algorithm is the lesser need for memory. This is even more vivid when we weigh BEM-LDC over uniform global refinement. Even for a simple model problem on a PC with 512MB, H$= 0.5$ is the minimum yet on the same PC we could go up to h$= 0.125$ using the BEM-LDC algorithm.

3.2 Practical example, the ICCP problem

In this section we solve a model problem of the Impressed Current Cathodic Protection (ICCP) system problem using the BEM-LDC algorithm. The results are compared to the solution obtained using a uniform grid. The ICCP is a system to prevent bare steel surfaces from corroding. One popular area of application is in submarines. Electrodes are attached to the surface of a ship and current flowed from and to the ship through water by applying a potential at these electrodes, see Fig. 11.

Fig. 11 : Part of a ship's surface for which ICCP is employed showing an electrode.

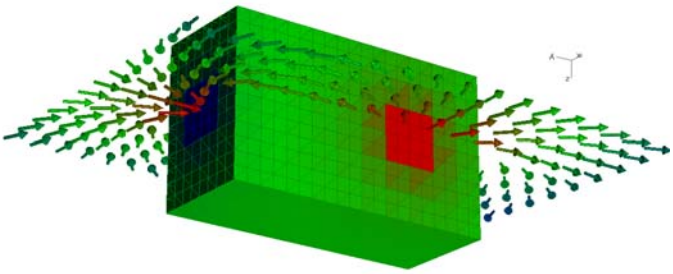

Fig. 12 : The potential and the normalised electric field vectors. The colour variation denotes a variation in the electric field strength for the arrows and the potential size on the box surface.

The current reverses the electrolysis reactions thus preventing corrosion. One is interested in calculating the potential and/or the electric field distribution in the water. In its simplest form, the problem is modeled as an exterior potential problem as follows. The ship is represented as a box with two small surfaces to model the electrodes. The box is then assumed to be totally submerged in water whose conductivity is assumed to be uniform. Apart from the electrodes, the rest of the ship's surface is painted and assumed to be perfectly insulating. We solve the problem with linear boundary conditions. Potentials u_a and u_c are assumed at the anode and cathode respectively. The potential in the water satisfies the Laplace equation. In summary we have the following model: Let u be the potemtial outside the box and $\mathbf{r}$ the position vector at a point in space, then

$$\begin{cases} \nabla^2 u(\boldsymbol{r}) = 0 & \boldsymbol{r} \in \Omega, \\ u(\boldsymbol{r}) = u_a & \boldsymbol{r} \in \partial\Omega_1, \\ u(\boldsymbol{r}) = u_c & \boldsymbol{r} \in \partial\Omega_2, \\ \dfrac{\partial u}{\partial n}(\boldsymbol{r}) := q(\boldsymbol{r}) = 0 & \boldsymbol{r} \in \partial\Omega \backslash \{\partial\Omega_1 \cup \partial\Omega_2\}, \end{cases} \tag{32}$$

where,

$$\Omega = \mathcal{R} \backslash \Omega^c$$
$$\Omega^c = \{\boldsymbol{r} : \boldsymbol{r} \in [0,4] \times [0,10] \times [0,6]\}$$
$$\partial\Omega_1 = \{\boldsymbol{r} : 1 \le x \le 3, y = 10, 2 \le z \le 4\}$$
$$\partial\Omega_2 = \{\boldsymbol{r} : x = 4, 2 \le y \le 4, 2 \le z \le 4\}$$

Thus we have steep gradients of the potential only at the electrodes. Let $u_a = 0.5$ and $u_c = -0.5$. The discretisation used is similar to the one in the first example above. The electric field distribution calculated is shown in Fig 12.

For the purpose of this paper details of the electric field calculation are omitted. In Tab. 2 we compare results obtained using uniformly refined grids to those of the BEM-LDC algorithm taking the anode as the active region. From the table we see that the results of the BEM-LDC algorithm are in agreement with those of uniformly refined grids in capturing the highly changing potential gradients.

4 Conclusions

In this paper we have presented an LDC technique for the BEM. LDC is an iterative process suitable for efficiently solving problems characterised by a region of high activity that covers a small part of the boundary for the physical domain. Examples are the Impressed Current Cathodic Protection problems such as those discussed in Kakuba (2005) and the thermoelastic problems discussed in Shiah, Guao, and Tan (2005). The problem is first solved on a global coarse grid, the computed coarse grid solution forms part of the boundary condition for a local problem defined in the active region where a more accurate solution is computed using a fine grid. The global coarse grid solution and the local fine grid solution are combined in a special way in an iterative manner through defect correction to improve the first coarse grid approximation. The new coarse grid approximation can in turn provide a boundary condition for a new local

Tab. 2 : Application example results: The solution at selected nodes on the surface. Nodes $1,\ldots,7$ are respectively (4.0,1.33,2.67), (4.0,0.67,3.33), (4.0,3.33,2.67), (4.0,2.67,3.33), (4.0,5.33,2.67), (4.0,4.67,3.33), (4.0,6.67,3.33). The BEM-LDC algorithm has been used with local problems of grid size h.

node	x	solution on uniform grid			BEM-LDC solution with H=2.0 as coarse grid	
		H=2.0	H=1.0	H=0.5	h=1.0	h=0.5
1	u	0.1593	0.1749	0.1868	0.1068	0.1061
2	u	0.0995	0.1084	0.1141	0.0661	0.0657
3	q	-0.5057	-0.3539	-0.3399	-0.3443	-0.3506
4	q	-0.5042	-0.3532	-0.3392	-0.3467	-0.3389
5	u	0.0948	0.1064	0.1129	0.0594	0.0595
6	u	0.1558	0.1729	0.1851	0.1018	0.1020
7	u	0.0383	0.04396	0.0462	0.0186	0.0186

problem. The process is repeated till convergence, which is in general very fast. Results of numerical experiments show that BEM-LDC can achieve the same accuracy as a uniform grid solver whose grid size coincides with that used in the local problem of BEM-LDC algorithm. But BEM-LDC guarantees a lower computational cost than the uniform grid solver.

References

Anthonissen, M. J. H. (2001): *Local Defect Correction Techniques: Analysis and Application to Combustion*. PhD thesis, Eindhoven University of Technology, Eindhoven, Netherlands, 2001.

Boersma, B.; Kooper, M. N.; Niewstadt, F. T. M.; Wesseling, P. (1997): Local grid refinement in large-eddy simulations. *Journal of Engineering Mathematics*, vol. 32, pp. 161 – 175.

Ferket, P. J. J.; Reusken, A. A. (1996): Further Analysis of the Local Defect Correction Method. *Computing*, vol. 56, pp. 117 – 139.

Hackbusch, W. (1984): Local defect correction method and domain decomposition technique. *Computing [Suppl.]*, vol. 5, pp. 89 – 113.

Kakuba, G. (2005): The Impressed Current Cathodic Protection System. Master's thesis, Eindhoven University of Technology, Eindhoven, Netherlands, 2005.

Ma, J.; Lu, H.; Komanduri, R. (2005): Structured mesh refinement in generalised interpolation material point (gimp) method for simulation of dynamic problems. *CMES: Computer Modeling in Engineering and Sciences*, vol. 12, pp. 213 – 227.

Paris, F.; Canas, J. (1997): *Boundary Element Method: Fundamentals and Applications*. Oxford University Press, Oxford.

Pozrikidis, C. (1992): *Boundary integral and singularity methods for linearised viscous flow*. Cambridge University Press.

Pozrikidis, C. (2002): *A Practical Guide to Boundary Element Methods with the software BEMLIB*. Chapman & Hall/CRC, London.

Shiah, Y.; Guao, T. L.; Tan, C. L. (2005): Two-dimensional bem thermoelastic analysis of anisotropic media with concentrated heat sources. *CMES: Computer Modeling in Engineering and Sciences*, vol. 7, pp. 321 – 338.